



Outgrowing seizures in Childhood Absence Epilepsy: time delays and bistability

Yue Liu^{1,2} · John Milton³ · Sue Ann Campbell⁴ 

Received: 16 July 2018 / Revised: 14 December 2018 / Accepted: 29 January 2019 / Published online: 9 February 2019
© Springer Science+Business Media, LLC, part of Springer Nature 2019

Abstract

We formulate a conductance-based model for a 3-neuron motif associated with Childhood Absence Epilepsy (CAE). The motif consists of neurons from the thalamic relay (TC) and reticular nuclei (RT) and the cortex (CT). We focus on a genetic defect common to the mouse homolog of CAE which is associated with loss of GABA_A receptors on the TC neuron, and the fact that myelination of axons as children age can increase the conduction velocity between neurons. We show the combination of low GABA_A mediated inhibition of TC neurons and the long corticothalamic loop delay gives rise to a variety of complex dynamics in the motif, including bistability. This bistability disappears as the corticothalamic conduction delay shortens even though GABA_A activity remains impaired. Thus the combination of deficient GABA_A activity and changing axonal myelination in the corticothalamic loop may be sufficient to account for the clinical course of CAE.

Keywords Childhood absence epilepsy · Time delay

1 Introduction

One of the outstanding questions in computational neuroscience concerns the identity of the mechanisms for seizure generation in patients with epilepsy (Eissa et al. 2017; da Silva et al. 2002, 2003; Jirsa et al. 2014; Milton et al. 2017;

Soltesz and Staley 2008; Weiss et al. 2013). Potential applications include the development of better methods to predict seizure recurrence (Milton et al. 1987; Osorio et al. 2010) and to abort seizures as they occur using carefully honed electrical stimuli (Milton and Jung 2003; Nagaraj et al. 2015). Consequently, current research has begun to focus on those epilepsies for which triggers for seizure onset, and sometimes seizure abortion, have already been identified (Osorio et al. 2011). This communication focuses on one such epilepsy, namely childhood absence (“3 Hz spike-and-wave”) epilepsy (CAE) (Milton et al. 2017). Other examples include nocturnal frontal lobe epilepsy (Quan et al. 2011) and the reflex epilepsies (Koepp et al. 2016). For these epilepsies it becomes possible, at least in principle, to directly compare observation to prediction not only in animal homologs, but in humans as well.

CAE is a familial epilepsy in which seizures typically begin between the ages of 4–6 years (Berkovic 1993). The seizures are typically short in duration (~ 9s; Penry et al. 1975) and manifest themselves as sudden cessation of movement with impaired consciousness (for example, staring blankly) followed by an abrupt return to normal behavior. Hence the term “absence”. A variety of molecular defects have been identified in CAE (Crunelli and Leresche 2002), most commonly located in subunits of the GABA_A (Wallace et al. 2001) and voltage-gated Ca⁺⁺ ion channels (Chen et al. 2014). In monozygotic twins, the

Action Editor: David Terman

✉ Sue Ann Campbell
sacampbell@uwaterloo.ca

Yue Liu
liuyue@math.ubc.ca

John Milton
JMilton@kecksci.claremont.edu

¹ Department of Applied Mathematics, University of Waterloo, Waterloo ON N2L 3G1, Canada

² Present address: Institute of Applied Mathematics and Department of Mathematics, University of British Columbia, Vancouver BC V6T 1Z2, Canada

³ W.M. Keck Science Department, The Claremont Colleges, Claremont, CA 91711, USA

⁴ Department of Applied Mathematics and Centre for Theoretical Neuroscience, University of Waterloo, Waterloo ON N2L 3G1, Canada

concordance does not reach 100% implying a small role for environmental factors (Berkovic 1993).

The electroencephalogram (EEG) recorded using scalp electrodes during an absence seizures shows widespread, bilaterally synchronous ~ 3 Hz spike-and-wave activity. Epileptic seizures are traditionally classified by the activity observed in EEG recordings during the onset of a seizure. Widespread electrographic activity at seizure onset corresponds to a generalized seizure while activity which is localized in a particular region at seizure onset is called a focal seizure. From this point of view the seizures in CAE are primary generalized seizures. However, with modern technologies including the magnetoencephalogram, it has become clear that absence seizures have a focal cortical onset: layer VI of somatosensory cortex in a rodent homolog of CAE (Meeren et al. 2002; Pollack et al. 2007), multiple cortical regions in humans with CAE (Gupta et al. 2011; Tenney et al. 2013; Westmije et al. 2009). Thus it is more accurate to classify absence seizures in CAE as focal onset with rapid secondary generalization, namely as secondarily generalized seizures. This distinction is important because it means that the onset, maintenance and cessation of seizures in CAE are controlled by an “epileptic system” that involves the interplay between cortical and subcortical neurons (Chkhenkeli and Milton 2003; Milton and Jung 2003; Milton et al. 2007). Indeed, effective generalization of seizure activity is not possible without the participation of the thalamus, cingulum and mesencephalon (Chkhenkeli and Milton 2003; Kreindler 1965; Weir 1964). In CAE the epileptic system takes the form of reciprocal interactions between cortical neurons (CT) and two nuclei located in the thalamus, namely the thalamic relay (TC) and reticular (RT) nuclei. The importance of this three neuron motif, shown in Fig. 1, for CAE seizure generation has been established in numerous studies (Breakspear et al. 2006; Chen et al. 2017; Destexhe 1998, 2008; Robinson et al. 2002; Suffczynski et al. 2004).

Much insight into CAE has been obtained through experimental work on animal homologs, that is, animals which spontaneously exhibit seizures with the same EEG signature as CAE. It has been shown that the common mouse homolog exhibits a defect in the α_1 subunit of the GABA_A receptors (Maljevic et al. 2006; McKusick 2017; Zhou et al. 2015), which results in a decreased GABA_A conductance. In the thalamus, only the TC neurons have α_1 subunit (Hortnagl et al. 2013), thus the expected effect of this defect is to reduce the inhibition felt by the TC neurons due to the RT neurons. One rat homolog exhibits abnormal behaviour of the T-type Ca²⁺ channels of the RT neurons. Electrophysiological experiments show an increase in conductance (Tsakiridou et al. 1995) of these channels. Recent work has shown there is a genetic defect which results in a decrease in the time constant of

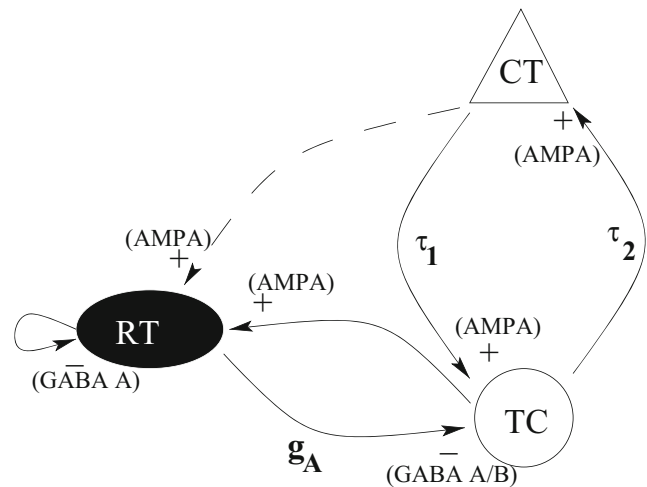


Fig. 1 Three neuron motif consisting of thalamic relay (TC) and thalamic reticular (RT) and cortical (CT) neurons. The main parameters important in this study are indicated. A self-feedback loop on RT accounts for the ability of RT neurons to inhibit other RT neurons. The connection between RT and CT is dashed since it is not included in this modeling study. See Section 2.1 for more details

inactivation, resulting in larger spikes during bursts (Powell et al. 2009). It is proposed that such changes would lead to an increase in synchronization between various TC neurons in the thalamocortical circuit (Tsakiridou et al. 1995) giving rise the spike-and-wave EEG activity of CAE.

Here we focus on the importance of two clinical observations for understanding the dynamics of the 3-neuron CAE motif. First, absence seizures can be triggered by hyperventilation and photic or auditory stimulation (Hogan and Sundram 1989). Often the seizures can be aborted by sensory stimuli, e.g. a sudden sound, or by gently shaking the patient. These clinical observations are suggestive of an underlying multistable dynamical system in which switches occur between different basins of attraction (Fan et al. 2016; Jirsa et al. 2014; da Silva et al. 2002, 2003; Milton 2000; Suffczynski et al. 2004). Second, there is the tendency for children with CAE to “outgrow” their epilepsy (Berkovic 1993; Milton et al. 2017). On reaching adulthood many patients with CAE no longer require anticonvulsant medications to remain seizure free, while others are able to control their seizures with reduced levels of medications. The fact that seizures can disappear even though the molecular defect persists strongly suggests that other factors must be involved in seizure generation. One possibility is that certain ion channel genes may be expressed in an age-specific way (Chen et al. 2014).

Another factor which changes as the brain matures is axonal myelination. Indeed, it has been pointed out that the clinical course of CAE seems to follow the active period for axonal maturation which nears completion by

mid to late adolescence (Milton et al. 2017). That is, the disappearance of seizures in adolescence could be attributed to a loss of multistability in the network due the reduction of conduction time delays. This is reminiscent of the properties exhibited by neural oscillators that are influenced by time-delayed pulsatile coupling (Foss et al. 1996, 1997; Foss and Milton 2000; Ma and Wu 2007). In these examples, multistability becomes possible when the time delay, τ , becomes longer than the intrinsic period, T , of the neural oscillator. This behavior has been demonstrated using a conductance based model of a delayed recurrent inhibitory loop (Ma and Wu 2007). Here we use numerical simulations to demonstrate that the same behaviors arise in a conductance based model of the 3-neuron motif shown in Fig. 1.

Our paper is organized as follows. First we develop a time-delayed conductance-based model for the neuronal motif shown in Fig. 1 using experimental observations obtained for the mouse homolog of CAE described above. We find that the periodic bursting dynamics generated by the interaction between the reticular (RT) and thalamic relay (TC) neurons within the thalamus (Destexhe 1998, 2008) is insensitive to changes in the conductance of the GABA_A channel. Moreover there is no bistability. Next we connect this 2-neuron circuit to a cortical neuron to form a 3-neuron circuit with delay. The combination of low GABA_A mediated inhibition of TC neurons and the long corticothalamic loop delay gives rise to a variety of complex dynamics including bistability. This bistability disappears as the corticothalamic conduction delay shortens even though GABA_A activity remains impaired. Thus the combination of deficient GABA_A activity and changing axonal myelination in the corticothalamic loop may be sufficient to account for the clinical course of CAE.

2 Materials and methods

All computer simulations were implemented with XPPAUT (Ermentrout 2002) using a 4th-order Runge-Kutta algorithm with a fixed step size. Source code is available in ModelDB (McDougal et al. 2017) at <http://modeldb.yale.edu/247704>.

2.1 3-neuron CAE motif

In view of studies on the mouse homolog for CAE the 3-neuron motif shown in Fig. 1 is different than in some other studies. First, we eliminate the connection between CT and RT neurons (dashed line) since optogenetic studies (Paz et al. 2011) diminish the importance of the feedforward inhibition component of the loop. We also note that the RT GABA_A receptors do not contain an α_1 subunit (Hortnagl et al. 2013). Since genetic defects in this subunit are

associated with CAE in mice, in our study only the GABA_A conductance on the TC neurons will be varied.

2.2 Conductance-based model

The neurons in Fig. 1 are modeled as conductance-based (Hodgkin-Huxley type) neurons (Ermentrout and Terman 2010; Hodgkin and Huxley 1952), and are based on previous work on the thalamocortical loop (Destexhe 1998, 2008; Destexhe et al. 1998).

The equations of the membrane potential, V , take the form

$$\begin{aligned} C_{TC} \frac{V_{TC}}{dt} &= -I_L - I_{Na} - I_K - I_T - I_h - I_{K2} - I_{synaptic}^{TC} + I_{ext}^{TC} \\ C_{CT} \frac{V_{CT}}{dt} &= -I_L - I_{Na} - I_K - I_M - I_{synaptic}^{CT} + I_{ext}^{CT} \\ C_{RT} \frac{V_{RT}}{dt} &= -I_L - I_{Na} - I_K - I_{TS} - I_{synaptic}^{RT} + I_{ext}^{RT} \end{aligned} \quad (1)$$

where $C_{TC} = C_{CT} = C_{RT} = 1\mu F/cm^2$ is the membrane capacitance (Destexhe et al. 1998) and the units for the membrane potential is mV. The intrinsic membrane currents include an external current (I_{ext}), a leak current (I_L), a transient voltage-gated Na⁺ current (I_{Na}), a transient voltage-gated K⁺ current (I_K), a low-threshold Ca⁺⁺ current (I_{TS}), a depolarization-activated K⁺ current (I_M), a low-threshold Ca⁺⁺ current (I_T), a mixed Na⁺-K⁺ current activated by hyperpolarization current (I_h) and a slow K⁺ current (I_{K2}) (Destexhe 2008; Destexhe and Babloyantz 1991; Destexhe et al. 1993, 1998). The external currents, I_{ext} 's, represent input from other brain regions (Behrens et al. 2003), and possibly brainstem (Weir 1964), which trigger activity in the motif. Without synaptic coupling, each of the three cells is at rest when their respective external current is zero and exhibit periodic spiking for a large range of nonzero values of external current input. With the parameters given in the Appendix the rheobases are 1.04 $\mu A/cm^2$ (CT neuron), 1.78 $\mu A/cm^2$ (TC neuron) and 0.40 $\mu A/cm^2$ (RT neuron). Although it is clear that I_{ext} can be quite complex, for most simulations we used $I_{ext}^{TC} = 5$ or $6 \mu A/cm^2$ and $I_{ext}^{CT} = I_{ext}^{RT} = 0 \mu A/cm^2$ and assume that this input is turned on at $t = 0$. To confirm the presence of multistability we added a 0.5s long $1.0\mu A/cm^2$ amplitude square wave perturbation to I_{ext}^{TC} .

The synaptic current for the neurons in the microcircuit are

$$I_{synaptic}^{TC} = I_{CT,AMPA} + I_{RT,GABA_A} + I_{RT,GABA_B} \quad (2)$$

$$I_{synaptic}^{CT} = I_{TC,AMPA} \quad (3)$$

$$I_{synaptic}^{RT} = I_{RT,GABA_A} + I_{TC,AMPA} \quad (4)$$

The AMPA and GABA_A synaptic currents have the general form (Destexhe et al. 1998)

$$I_{\text{syn}} = \bar{g} s(t) (V_{\text{post}} - E_{\text{syn}})$$

where E_{syn} is the reversal potential, \bar{g} is the (constant) maximal conductance and s is the fraction of ion channels that are open due to neurotransmitter released by the presynaptic neuron. This follows the model

$$\frac{ds}{dt} = \alpha T(t)(1 - s) - \beta s \quad (5)$$

where α, β are constants that depend only on the type of neurotransmitter and T is the concentration of transmitter released given by

$$T(t) = \frac{2.84}{1 + \exp\left(\frac{2 - V_{\text{pre}}(t)}{5}\right)} \quad (6)$$

The excitatory neurotransmitter is glutamate and the membrane receptor is the ionotropic transmembrane AMPA (α -amino-3-hydroxy-5-methyl-4-isoxazolepropionic acid) receptor. For I_{AMPA} the parameter values in our model are: $E_{\text{AMPA}} = 0$ mV, $\alpha_{\text{AMPA}} = 0.94$ ms⁻¹mM⁻¹, and $\beta_{\text{AMPA}} = 0.18$ ms⁻¹ (Destexhe et al. 1994, 1996). For the GABA_A current the parameter values are $E_{\text{GABA}_A} = -85$ mV, $\alpha_{\text{GABA}_A} = 5$ ms⁻¹mM⁻¹, and $\beta_{\text{GABA}_A} = 0.18$ ms⁻¹.

The I_{GABA_B} current was modeled as (Destexhe et al. 1996)

$$I_{\text{GABA}_B} = \bar{g}_{\text{GABA}_B} \frac{s^4}{s^4 + K_d} (V_{\text{post}} - E_{\text{GABA}_B}) \quad (7)$$

$$\frac{dr}{dt} = 0.5T(t)(1 - r) - 0.0012r \quad (8)$$

$$\frac{ds}{dt} = 0.18r - 0.034s \quad (9)$$

where r represents the GABA_B receptor, s the synaptic gating variable, $T(t)$ is given by Eq. 6 and $E_{\text{GABA}_B} = -95$ mV.

The maximal synaptic conductances are given in Table 1. These are based on values in Destexhe et al. (1996) adjusted to account for the smaller network structure.

Table 1 Maximal synaptic conductances used in the model

type	location	\bar{g} (mS/cm ²)
AMPA	TC→CT	4.138
	CT→TC	0.1
	TC→RT	1.428
GABA _A	RT→TC	0.1 – 0.7
	RT→RT	6
GABA _B	RT→TC	0.13793

2.3 Time delay

It is important to distinguish between the effects of a lag and a time delay on the dynamics of a neural circuit (Milton and Ohira 2014). The response of a model described by ordinary differential equation to an input lags behind the time course of the stimulus. In other words, the time course of the stimulus overlaps that of the response. Thus, the synaptic dynamics described by Eq. (5) or Eqs. (8)–(9) contribute a lag to the dynamics, related to the rise time and decay of the potential due to activity in the synapse.

In the case of a time delay, there is a clear separation in time between the stimulus and the response. For example, the separation between when the action potential is generated at the axon hillock and the subsequent release of neurotransmitter into the synaptic cleft. This separation between stimulus and response arises because the axonal conduction velocity is finite. Here we model this by including an explicit dependence on a delayed value of the voltage of the presynaptic neuron. We include two conduction delays: the corticothalamic delay, τ_1 , and thalamocortical delay, τ_2 . Thus for the AMPA synapse from the CT neuron to the TC neuron (6) becomes

$$T(t) = \frac{2.84}{1 + \exp\left(\frac{2 - V_{\text{CT}}(t - \tau_1)}{5}\right)} \quad (10)$$

while for the AMPA synapse from the TC neuron to the CT neuron we have

$$T(t) = \frac{2.84}{1 + \exp\left(\frac{2 - V_{\text{TC}}(t - \tau_2)}{5}\right)} \quad (11)$$

The thalamocortical delay, τ_2 , measured using depth electrodes in a child with CAE (Williams 1953) and in adults undergoing invasive monitoring for evaluation for epilepsy surgery (Mak-McCully et al. 2017) is 14 ms. Thus this delay does not change as the brain matures. The thalamocortical delay is ~ 25% of the total corticothalamic loop delay (Hashemi et al. 2017; Roberts and Robinson 2008), suggesting that the corticothalamic delay, τ_1 , is ~ 42 ms. A similar difference between the thalamocortical and corticothalamic delay has been observed experimentally in several species (Roberts and Robinson 2008) and is attributed to larger conduction velocities in thalamic axons vs cortical axons (Swadlow and Waxman 2012).

Since all of the parameters used in Eq. (1) have been determined for mouse and rats it is necessary to modify the delay to account for the smaller brains of rodents. The distance between the thalamus and brain in a rat and mouse is ~ 1 cm and in a human is about ~ 5 cm. Thus for a rodent the estimated thalamocortical delay becomes ~ 2.8 ms and the corticothalamic delay in an rodent with absence seizures would be ~ 8.4 ms.

Although time delays may exist between thalamic neurons, they are likely to be very short especially in relation to the lags introduced by the slow GABA_B receptors. In addition it is likely that gap junctions exist between the thalamic neurons (Beenhakker and Huguenard 2009; Landisman et al. 2002). Therefore we assumed that all conduction delays between intrathalamic neurons were equal to 0 ms.

2.4 Initial conditions

The distinction between a time delay and a lag has important consequences for the determination of the initial conditions for (1) (Milton and Ohira 2014). Since a lag is modeled by an ordinary differential equation, it is only necessary to specify the initial conditions at a single instance in time, t_0 . On the other hand, the presence of a conduction time delay, τ , means that the model becomes a delay differential equation and the initial condition becomes an initial function $\Phi(t)$ where $t \in [t_0 - \tau, t_0]$. Hence the initial condition space for a delay differential equation is a function defined on the interval $[-\tau, 0]$. Here we have two time delays so $\tau = \max(\tau_1, \tau_2)$.

For most simulations we kept the initial functions for the RT and CT neurons constant at the resting equilibrium values

$$\Phi_{RT}(t) = -89.40\text{mV} \quad \text{for } t \in [-\tau, 0]$$

$$\Phi_{CT}(t) = -70.56\text{mV} \quad \text{for } t \in [-\tau, 0]$$

and varied the initial function for the TC neuron as

$$\begin{aligned} \Phi_{TC}(t) &= -76.74\text{mV} \quad \text{for } t \in [-\tau, 0] \\ &= V_X(0) \quad \text{for } t = 0 \end{aligned}$$

Seven choices of $V_X(0)$ were used to test for bistability: 0 mV, ± 20 mV, ± 40 mV, ± 60 mV. We also considered initial conditions which corresponded to all the cells be slightly depolarized

$$\Phi_{RT}(t) = -73.23\text{mV} \quad \text{for } t \in [-\tau, 0]$$

$$\Phi_{CT}(t) = -61.26\text{mV} \quad \text{for } t \in [-\tau, 0]$$

$$\Phi_{TC}(t) = -29.26\text{mV} \quad \text{for } t \in [-\tau, 0]$$

As the gating functions only require initial conditions at $t = 0$ these were set to correspond to the values of the (appropriate) voltage at $t = 0$.

3 Results

We interpret the three neuron motif shown in Fig. 1 as a neural oscillator formed by the RT-TC neurons under the influence of a delayed recurrent excitatory loop formed by the connections between CT and TC neurons. Our goal is

to examine the behavior of this circuit as two parameters, namely the maximal conductance, \bar{g}_A , for the GABA_A mediated inhibition on TC neurons by RT neurons and the conduction time delay, τ_1 , between CT and TC neurons are varied. All other parameters are held constant and are summarized in Section 2.2 and the Appendix.

3.1 RT-TC oscillator

When a constant current is injected into the TC neuron, the RT-TC motif exhibits two modes of rhythmic oscillation. If the current amplitude is less than $\sim 5.6 \mu\text{A}/\text{cm}^2$, the circuit exhibits a slow (several Hz) periodic discharge. This rhythm is characterized by bursting of the RT neuron (black) with the TC neuron (red) firing one spike per RT burst. The frequency of this oscillation slowly changes with the amplitude of the applied current, I_{TC} , and is not strongly dependent on the strength of the GABA_A conductance, \bar{g}_A , input from the RT neuron to the TC neuron over the range $0.1 - 0.7 \text{ mS}/\text{cm}^2$. See the left two panels of Fig. 2.

If the injected current amplitude is greater than $\sim 5.6 \mu\text{A}/\text{cm}^2$, the rhythm is tonic spiking in which both the TC and RT neurons have one spike per period. The frequency of this rhythm rapidly changes with the strength of the applied current and is strongly dependent on \bar{g}_A . See the right two panels of Fig. 2.

The complexity of the dynamics of the RT-TC-CT motif, as we shall see later in Section 3.2 is, in part, related to the applied current and \bar{g}_A dependent responses of the RT-TC motif. Figure 3 shows the effect of applying a 0.5s long, $1 \mu\text{A}/\text{cm}^2$ square wave pulse of current to the TC neuron which is also receiving a $5 \mu\text{A}/\text{cm}^2$ tonic current input (total TC neuron current input in the RT-TC motif is $6.5 \mu\text{A}/\text{cm}^2$). The response of the RT-TC motif to the square wave pulse current is to produce a fast tonic spiking mode which terminates when the current pulse is over. Further, as shown in the figure, the frequency of spiking during the current pulse increases as \bar{g}_A increases. This behavior is consistent with the observation that a novel stimulus can change thalamic neurons from a “burst mode” to a “tonic mode” (Kandel et al. 2000).

3.2 RT-TC-CT delayed recurrent excitatory loop

We next added the CT neuron to make the RT-TC-CT motif. The CT neuron responds to an excitatory input with a burst of action potentials (typically 2). Figure 4 illustrates the rich variety of spiking patterns that occur in the 3-neuron CAE motif when $\tau_1 = 9\text{ms}$, $\tau_2 = 2.8\text{ms}$, $I_{\text{ext}}^{\text{TC}} = 5 \mu\text{A}/\text{cm}^2$ and \bar{g}_A is varied. These spiking patterns include regular and irregular bursting (Types 1 and 2) as well as rapid tonic spiking (Type 3). For convenience, the bursting patterns generated by the RT-TC-CT motif were further classified by

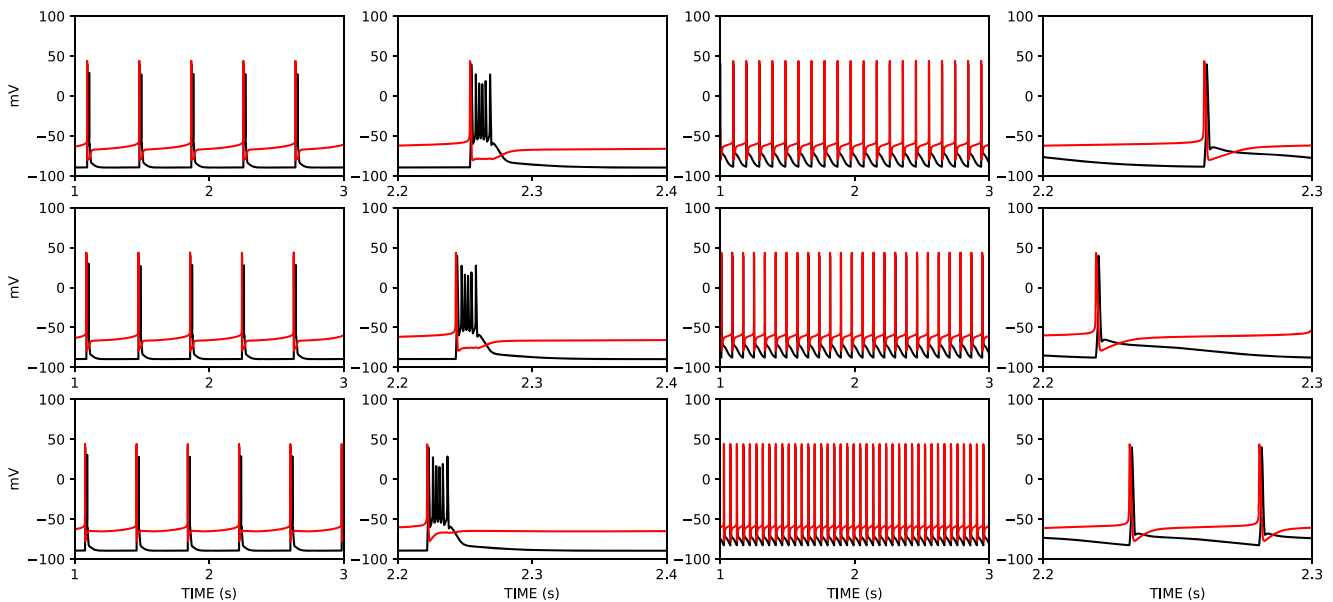


Fig. 2 Oscillation modes of the RT-TC motif. The motif exhibits bursting for $I_{ext} < 5.6 \mu\text{A}/\text{cm}^2$ and tonic spiking for $I_{ext} > 5.6 \mu\text{A}/\text{cm}^2$. Left two columns: $I_{ext}^{TC} = 5 \mu\text{A}/\text{cm}^2$, right two columns: $I_{ext}^{TC} = 6 \mu\text{A}/\text{cm}^2$. Variation of the GABA_A conductance from RT to TC has

minimal effect on the bursting rhythm and a strong effect on the tonic rhythm. Top row: $\bar{g}_A = 0.6 \text{ mS}/\text{cm}^2$, middle row: $\bar{g}_A = 0.3 \text{ mS}/\text{cm}^2$, bottom row: $\bar{g}_A = 0.1 \text{ mS}/\text{cm}^2$. All other parameters are given in Section 2 and the Appendix. Black is RT neuron; Red is TC neuron

the behavior of V_{RT} which followed the initial, short burst of action potentials. For Type 1, V_{RT} returns to its resting value. For Type 2 solutions V_{RT} remains depolarized after the initial burst of spikes for varying lengths of time: Type 2a is followed by a single action potential, for Type 2b there is a train of action potentials organized into a regular bursting pattern of varying lengths, and for Type 2c there is an irregular bursting pattern.

We carried out extensive numerical simulations of the model varying the maximal conductance, \bar{g}_A , of the GABA_A synapse on the TC neurons in the range $0.1 - 0.7 \text{ mS}/\text{cm}^2$ and the time delay, τ_1 , from the CT neurons to the TC neurons in the range $2 - 9.2 \text{ ms}$. A range of initial conditions was explored including with all the neurons starting from rest and with the TC and CT neurons starting in various depolarized states. The results of the simulations are summarized in Fig. 5.

3.3 Bistability

For some large and small values of \bar{g}_A , only one type of rhythm was observed. In particular, for $\bar{g}_A = 0.7 \text{ mS}/\text{cm}^2$, the RT-TC-CT motif only exhibited the slow rhythm (Type 1 in Fig. 4) regardless of the size of the time delay. For values of \bar{g}_A in the range $0.1 - 0.2 \text{ mS}/\text{cm}^2$ one of Type 2a, 2b or 2c bursting rhythm was observed. These bursting rhythms have various numbers of spikes per burst.

As shown in Fig. 5, however, bistability occurred in two parameter regions. There was co-existence of Type 1 and Type 2a spiking patterns for \bar{g}_A in the range $0.3 - 0.4 \text{ mS}/\text{cm}^2$ and $\tau_1 \leq 5 \text{ ms}$ and co-existence of Type 1 and Type 3 spiking patterns when \bar{g}_A is in the range $0.3 - 0.6 \text{ mS}/\text{cm}^2$ and τ_1 in the range $5.6 - 9.2 \text{ ms}$. Since the inter-spike and burst frequencies for the Type 1 and Type 2a patterns were about the same we did not identify this bistability with

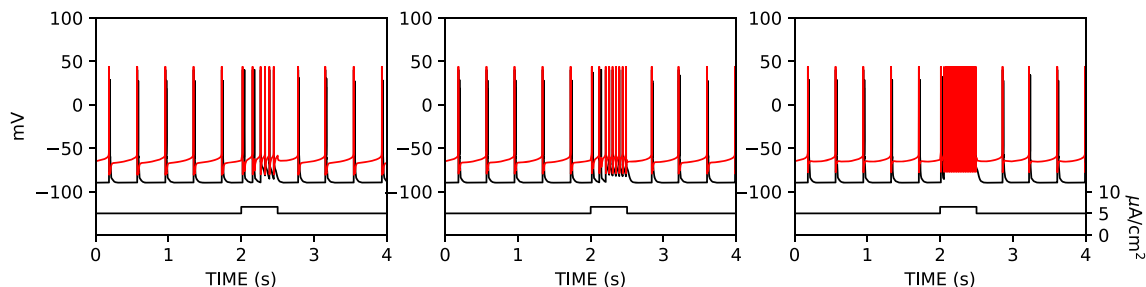
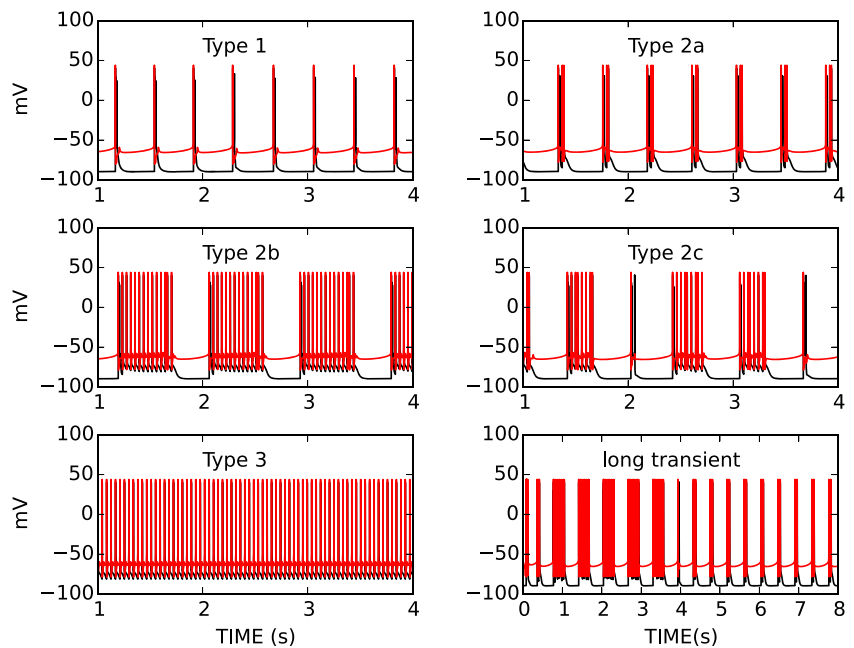


Fig. 3 Response of the RT-TC motif to a square wave perturbation in applied current. Input current (shown at bottom of plots) is $5 \mu\text{A}/\text{cm}^2$ except from $t = 2 \text{ s}$ to $t = 2.5 \text{ s}$ where it is $6.5 \mu\text{A}/\text{cm}^2$. Left: $\bar{g}_A = 0.1$

mS/cm^2 , middle: $\bar{g}_A = 0.4 \text{ mS}/\text{cm}^2$, right: $\bar{g}_A = 0.7 \text{ mS}/\text{cm}^2$. Black is RT neuron. Red is TC neuron

Fig. 4 Variety of spiking patterns in the RT-TC-CT motif with CT-TC delay of 9ms, TC-CT delay of 2.8ms, $I_{ext}^{TC} = 5\mu A/cm^2$ and varying TC-RT $GABA_A$ conductance, \bar{g}_A . Top left $\bar{g}_A = 0.6\text{ mS/cm}^2$, top right $\bar{g}_A = 0.1\text{ mS/cm}^2$, middle left $\bar{g}_A = 0.29\text{ mS/cm}^2$, middle right $\bar{g}_A = 0.25\text{ mS/cm}^2$, bottom left $\bar{g}_A = 0.4\text{ mS/cm}^2$, bottom right $\bar{g}_A = 0.2\text{ mS/cm}^2$. All other parameters are as described in Section 2 and the Appendix. Black is RT neuron; Red is TC neuron. For simplicity the voltage of the CT neuron is not shown



the bistability observed in CAE. Instead we identified the bistability observed between Type 1 and Type 3 spiking patterns with the behaviors observed in CAE.

Figures 6 and 7 illustrate our proposed clinical scenario. When \bar{g}_A is in the normal range there is no bistability and changes in τ_1 do not affect the spiking pattern of the RT-TC-CT motif (Fig. 6, left-hand panels). For this range of \bar{g}_A and any value of τ_1 in the biological range, the application of a short, square wave current pulse to the TC neuron only produced fast spiking as long as the pulse was

applied (Fig. 7, left-hand panels). In contrast, when \bar{g}_A is sufficiently lower than normal and τ_1 is long enough, there is bistability between the slow bursting rhythm and a state of high frequency tonic firing (Fig. 6, right-hand panels). In this case, the application of a brief square wave current pulse could switch the system from the bursting mode to the high frequency spiking mode (top right panel in Fig. 7). In this same range of \bar{g}_A , when τ_1 is decreased (bottom right panel) there is no bistability and the response of the RT-TC-CT motif to a square wave current pulse is similar to the “normal case” (left panels in Fig. 7). This is what we interpret as “outgrowing” the CAE seizures.

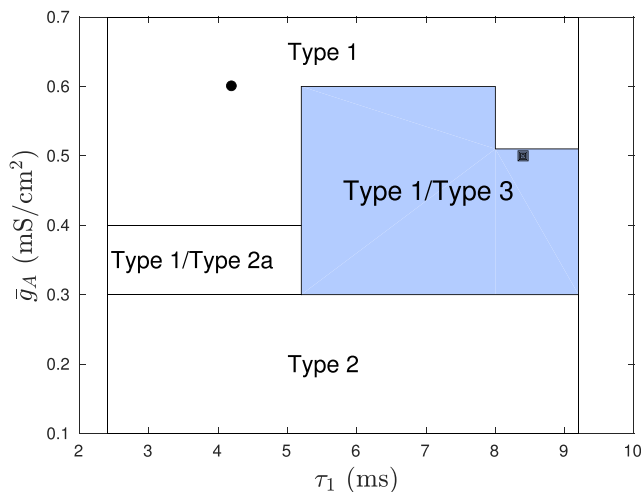
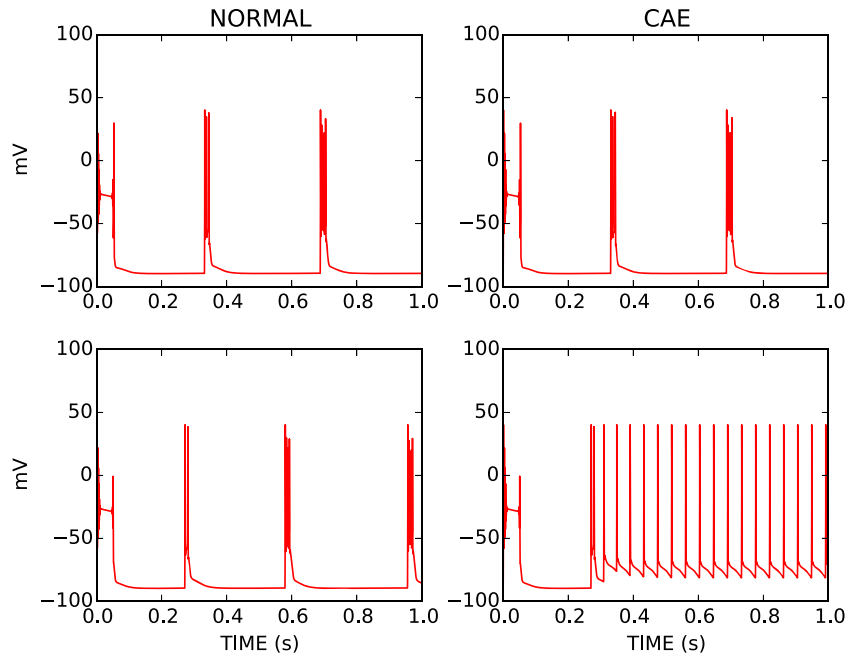


Fig. 5 Summary of the numerical simulations of the RT-TC-CT motif as a function of \bar{g}_A and τ_1 . In the region marked Type 2, one of Type 2a, 2b or 2c occurred. For examples of the spiking patterns see Fig. 4. The ● and ■ show parameter values used in the simulations shown in Fig. 6

4 Discussion

Current mathematical approaches to seizure generation are often motivated by the identification of the bifurcation that occurs at seizure onset and offset (Houssaini et al. 2015; Jirsa et al. 2014). However, time series analysis suggest less than 10% of seizure onsets have features suggestive of known bifurcations (Milanowski and Suffczynski 2016). Here we have focused on identifying a mechanism for the clinically observed bistability of seizures in CAE in terms of the properties of delayed recurrent loops. This approach draws attention to the connectivity between neurons, the timing of neural spikes and the conduction time delays between them. The effect of the time delays is to alter the timing in the interaction between neurons. Although we have emphasized the role played by recurrent loops between cortex and subcortical nuclei, it is quite possible that a similar scenario can arise between sufficiently separated

Fig. 6 Simulations of the model illustrating the behavior we interpret as normal and CAE. Left hand column: when \bar{g}_A is in the normal range, and any value of τ_1 , there is no bistability when $V_X(0)$ is changed. Top left: $V_X(0) = +20$ mV, bottom left: $V_X(0) = 0$ mV. Right hand column: when \bar{g}_A is not in normal range and τ_1 is sufficiently large there is bistability when $V_X(0)$ is changed. Top right: $V_X(0) = +20$ mV, bottom left: $V_X(0) = 0$ mV. Parameter values: $g_A = 0.6$ mS/cm² and $\tau_1 = 4.2$ ms (left column, ● in Fig. 5); $g_A = 0.5$ mS/cm² and $\tau_1 = 8.4$ ms (right column, ■ in Fig. 5). For simplicity, only the voltage of the TC neuron is shown



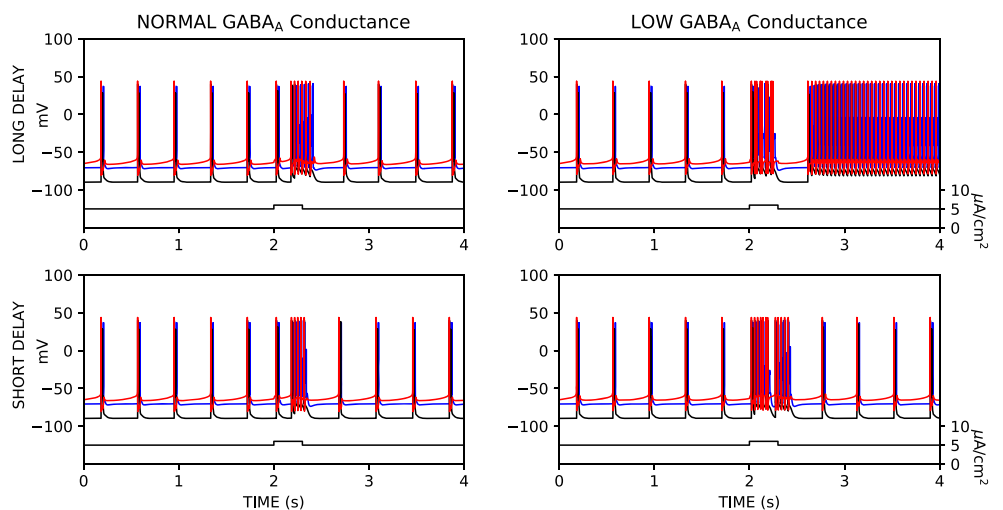
cortical regions interconnected by association and commissural fibers (Jirsa et al. 2017; Milton et al. 2007).

The effect of the time delay on the behaviors of the RT-TC-CT motif can be understood as follows. The two-neuron RT-TC circuit has two modes: slow bursting and tonic spiking. Which mode is observed depends on the strength of the input current into the TC neuron. In our simulations we chose the baseline input to correspond to the slow bursting mode. When the CT neuron is added to create the three neuron RT-TC-CT motif, it can provide more excitatory input to the TC neuron causing it to spike if the timing is right. In particular, CT input must arrive to TC neuron when it is not under inhibition by the RT neuron.

The input to the TC neuron induces a burst in the RT neuron and a burst (after a short time delay of 2.8 ms) in the

CT neuron. The CT neuron burst can in turn induce a TC neuron spike if the delay between CT and TC is long enough and/or the inhibition of RT is weak enough so that the TC neuron is no longer inhibited when it feels the effect of the CT neuron burst. This leads to the behavior summarized in Fig. 5. In particular, if the inhibition is strong enough (e.g. $\bar{g}_A = 0.7$), a single burst of CT is not enough to cause a spike in TC for the biologically plausible range of delays we explored. This leads to the Type 1 behavior where the RT-TC motif remains in the slow bursting rhythm and the effect of the CT neuron is negligible. On the other hand, if the inhibition is very weak ($\bar{g}_A = 0.1 - 0.2$), the CT burst can cause a second TC spike. This initiates a network burst where the TC and RT neurons spike multiple times and the CT neuron has multiple bursts, which we call Type

Fig. 7 Response of the RT-TC-CT circuit to a perturbation in applied current. Left: $\bar{g}_A = 0.7$ mS/cm², right: $\bar{g}_A = 0.4$ mS/cm². Top: $\tau_1 = 8.4$ ms, bottom: $\tau_1 = 2.8$ ms. Input current (show at bottom of plots) is $I_{ext}^{TC} = 5 \mu\text{A}/\text{cm}^2$, except from $t = 2.0$ s to $t = 2.3$ s where $I_{ext}^{TC} = 6 \mu\text{A}/\text{cm}^2$. Initial conditions are chosen so the system is on the slow bursting solution corresponding to $I_{ext}^{TC} = 5 \mu\text{A}/\text{cm}^2$. Black is RT neuron. Red is TC neuron. Blue is CT neuron. Other parameters are as given in Section 2 and the Appendix



2 behavior. The number of spikes depends on the level of inhibition and the size of the delay, but the overall bursting is not strongly dependent on these parameters.

For midrange values of \bar{g}_A , the behavior becomes strongly dependent on the delay. For small delay the system exhibits either Type 1 (stronger inhibition) or Type 2 (weaker inhibition) behavior. With large delay the system can exhibit bistability between the Type 1 and Type 3 behavior. In Type 3 the time delay from the CT and TC neuron creates a reverberation between the CT neuron and the RT-TC motif which is like a network burst with infinite period. In essence, the CT neuron is acting like a continuous additional input to the RT-TC motif which is pushing it into the fast spiking mode. Which behavior occurs is dependent on initial conditions.

Due to the complexity of the behavior it is difficult to classify this as a bifurcation at the level of the individual neurons. However if we consider the network averaged firing rate, then Type 3 behavior corresponds to a constant firing rate, while Type 2 corresponds to a periodically varying firing rate. Thus, the loss of Type 3 behavior with decreasing delay could be associated with a Hopf bifurcation of the firing rate.

We have attempted to choose values for the thalamocortical and corticothalamic time delays that are realistic for the mouse model of CAE, however, the mechanism we observe is robust to some variation in these values. We have carried out simulations with other ranges of values for the time delay and even allowed two delays to be the same. In all cases we found that low $GABA_A$ conductance with large enough time delay led to bistability between type 1 and type 3 behaviors.

While our three neuron motif is clearly a vastly over simplified representation of the thalamocortical system, we feel that the basic mechanism is likely to carry over to larger networks with the same connectivity structure and delays. It is a common theme that small motifs contain at least the germ of the behavior found in larger networks and can often be used to determine the mechanisms of behavior observed in larger networks (Destexhe 2008; Skinner et al. 2005). One phenomenon that our small motif model cannot address is how the parameter values affect the synchronization of neurons in a population. This could be addressed by coupling several of our motifs together. We leave this for future work.

Our work builds on past work on conductance-based models of the thalamocortical loop (Destexhe 1998, 2008; Destexhe et al. 1998). Our contribution is the incorporation of time delays, which lead to a natural mechanism (bistability) for seizures to spontaneously arise and disappear. Our work is complementary to the majority of other recent work which has focused on mean-field type models

representing the activity level of entire populations of neurons (Breakspear et al. 2006; Chen et al. 2017; Fan et al. 2016; Roberts and Robinson 2008; Robinson et al. 2002; Yang and Robinson 2017). We share with many of these models an emphasis on the importance of time delays in the generation of absence seizures. Our work has shown that these ideas carry over to models which incorporate detailed biophysical of individual neurons and elucidated the mechanisms involved in the bistability associated with time delay. Lower level models such as ours will be important to study other genetic defects associated with CAE, such as in calcium channels, which affect excitability and firing properties at the individual neuron level (Chen et al. 2014; Powell et al. 2009; Tsakiridou et al. 1995). We leave this study for future work.

Often overlooked is the role played by subcortical nuclei located in the thalamus, cingulum and brainstem in the maintenance, generalization and even termination of the seizure (Arakaki et al. 2016; Chkhenkeli and Milton 2003; Kreindler 1965). These subcortical nuclei are separated by a few centimeters from the location of typical cortical epileptic foci. As a consequence, the neurons in the epileptic system are pulse-coupled, namely the interactions between them take the form of discrete synaptic potentials driven by neural spikes. One paradigm which is simple enough for mathematical insight into these cross-scale neurodynamical systems is the delayed recurrent loop control of an oscillator (Foss et al. 1996, 1997; Foss and Milton 2000; Ma and Wu 2007). Here we have shown that the 3-neuron motif for CAE is equivalent to an oscillator formed by the interaction between intrathalamic neurons (RT and TC) and a delayed recurrent excitatory loop that involves corticothalamic interactions. Just as in the case of a delayed recurrent inhibitory loop, bistability arises in the delayed recurrent excitatory loop as the conduction delays become sufficiently long. We anticipate that similar behaviors will even be observed in a large neural network.

The thalamus has reciprocal connections with extensive regions of the cortex (Behrens et al. 2003). This is the anatomical basis for the roles that the thalamus plays, for example, in rapid seizure generalization and sleep (Kostopoulos 2000). It is tempting to identify the slow bursting mode of the RT-TC motif as the “baseline state” (sleeping/inattentive state) and the spiking mode as the “response to inputs”. From this point of view delayed feedback from one part of cortex can cause malfunction in the interactions between the RT and CT neurons so that it does not “turn off” its response to an input received from another area of cortex. If the input represented a seizure starting in a cortical epileptic focus, then this interaction could put in motion a delay-induced reverberation that maintains the seizure. The slow bursting mode of the RT-TC

motif might also lie at the basis of the central reaction time in motor control (van de Kamp et al. 2013; Vince 1948) and the focusing of attention (Crick 1984).

The importance of distinguishing between time delays and lags in models of spatially extended neural networks has received little systematic attention. When there is a clear distinction between the time that a stimulus is delivered and the time the response occurs, it is necessary to model the time difference as a time delay (Milton and Ohira 2014). This is how τ_1 was estimated (Roberts and Robinson 2008) and τ_2 was measured (Mak-McCully et al. 2017; Williams 1953). Even in the case of a metabotropic ion channel, such as GABA_A, there is a time delay involved, albeit very small. The numerical integration of neural networks with delay is demanding since the memory requirements rapidly increase as the number of time delays increase and the integration time step decreases. Thus it is tempting to approximate all delays as lags. When the time delay is very small compared to the characteristic times of the system (e.g. the e^{-1} time), this approximation can be mathematically justified (Driver et al. 1973; Kurzweil 1971). However, this approximation is not necessarily valid as the time delay becomes comparable to the system's characteristic response time (see, for example, Insperger 2015). In our investigation we purposely modeled delays within the thalamus as lags in order to focus our attention on the effects of time delays between thalamus and cortex on the dynamics exhibited by the RT-CT-TC motif. This is because our goal was to obtain insight into the tendency of seizures in CAE to decrease or even disappear with aging. The tendency to outgrow the epilepsy appears to correlate with increased cortical axonal myelination as the brain matures into adulthood (Milton et al. 2017). As we have shown, modeling this effect via a delay provides a possible explanation for this aspect of the clinical course of CAE.

Acknowledgments We thank Samuel Berkovic and Peter Camfield for useful comments on the clinical history and inheritance of children with CAE and Anthony Burre for help with the numerical simulations. SAC and YL acknowledge the support of the Natural Sciences and Engineering Research Council of Canada. JM acknowledges support from the William R Kenan, Jr Charitable Trust.

Compliance with Ethical Standards

Conflict of interests The authors declare that they have no conflict of interest.

Appendix: Intrinsic currents

We present here the details of the models for the intrinsic currents of the three neurons of the model (1).

Leak currents:

TC neurons (Destexhe et al. 1993, 1998): $I_L = \bar{g}_L(V - E_L)$; $\bar{g}_L = 0.01$ mS/cm² and $E_L = -70$ mV.

CT neurons (Destexhe et al. 1998): $I_L = \bar{g}_L(V - E_L)$; $\bar{g}_L = 0.1$ mS/cm² and $E_L = -70$ mV.

RT neurons (Destexhe et al. 1996): $I_L = \bar{g}_L(V - E_L)$; $\bar{g}_L = 0.05$ mS/cm² and $E_L = -90$ mV.

Transient voltage-gated K⁺ current (Traub and Miles 1991)

$$I_K = \bar{g}_K m_k^4 h_K (V - E_K) \quad (12)$$

$$\frac{dm}{dt} = \alpha_m(V)(1 - m) - \beta_m(V)m \quad (13)$$

$$\frac{dh}{dt} = \alpha_h(V)(1 - h) - \beta_h(V)h \quad (14)$$

$$\alpha_{m_k}(V) = \frac{0.032(15 - V)}{\exp(\frac{15-V}{5}) - 1} \quad (15)$$

$$\beta_{m_k}(V) = 0.5 \exp(\frac{10 - V}{40}) \quad (16)$$

$$\alpha_{h_k}(V) = 0.028 \exp(\frac{15 - V}{15}) + \frac{2}{\exp(\frac{85-V}{10}) + 1} \quad (17)$$

$$\beta_{h_k}(V) = \frac{0.4}{\exp(\frac{40-V}{10}) + 1} \quad (18)$$

TC neurons: $\bar{g}_K = 10$ mS/cm², $E_K = -90$ mV

CT neurons: $\bar{g}_K = 5$ mS/cm², $E_K = -90$ mV

RT neurons: $\bar{g}_K = 20$ mS/cm², $E_K = -80$ mV

Transient voltage-gated Na⁺ current (Traub and Miles 1991)

$$I_{Na} = \bar{g}_{Na} m_{Na}^3 h_{Na} (V - E_{Na}) \quad (19)$$

$$\frac{dm}{dt} = \alpha_m(V)(1 - m) - \beta_m(V)m \quad (20)$$

$$\frac{dh}{dt} = \alpha_h(V)(1 - h) - \beta_h(V)h \quad (21)$$

$$\alpha_{m_{Na}}(V) = \frac{0.32(13 - V)}{\exp(\frac{13-V}{4}) - 1} \quad (22)$$

$$\beta_{m_{Na}}(V) = \frac{0.28(V - 40)}{\exp(\frac{V-40}{5}) - 1} \quad (23)$$

$$\alpha_{h_{Na}}(V) = 0.128 \exp(\frac{17 - V}{18}) \quad (24)$$

$$\beta_{h_{Na}}(V) = \frac{4}{\exp(\frac{40-V}{5}) + 1} \quad (25)$$

for TC neurons: $\bar{g}_{Na} = 90$ mS/cm², $E_{Na} = +45$ mV

for CT neurons: $\bar{g}_{Na} = 50$ mS/cm², $E_{Na} = +45$ mV

for RT neurons: $\bar{g}_{Na} = 200$ mS/cm², $E_{Na} = +45$ mV

Low threshold Ca^{++} current (Huguenard and Prince 1992)

$$I_{TS} = \bar{g}_{\text{Ca}} m_{\text{TS}}^2 h_{\text{TS}} (V - E_{\text{Ca}}) \tag{26}$$

$$\frac{dm}{dt} = \frac{m_{\infty}(V) - m}{\tau_m(V)} \tag{27}$$

$$\frac{dh}{dt} = \frac{h_{\infty}(V) - h}{\tau_h(V)} \tag{28}$$

$$m_{\infty}(V) = \frac{1}{1 + \exp(\frac{-(V+52)}{7.4})} \tag{29}$$

$$\tau_m(V) = 1 + \frac{0.33}{\exp(\frac{V+48}{4}) + \exp(\frac{-(V+407)}{50})} \tag{30}$$

$$h_{\infty}(V) = \frac{1}{1 + \exp(\frac{V+80}{5})} \tag{31}$$

$$\tau_h(V) = 28.3 + \frac{0.33}{\exp(\frac{V+48}{4}) + \exp(\frac{-(V+407)}{50})} \tag{32}$$

where $\bar{g}_{\text{Ca}} = 3 \text{ mS/cm}^2$, $E_{\text{Ca}} = +120 \text{ mV}$.

Depolarization-activated K^+ current (McCormick et al. 1993)

$$I_{\text{M}} = \bar{g}_{\text{M}} m_{\text{M}} (V - E_{\text{M}}) \tag{33}$$

$$\frac{dm}{dt} = \frac{m_{\infty}(V) - m}{\tau_m(V)} \tag{34}$$

$$m_{\infty}(V) = \frac{1}{1 + \exp(\frac{-(V+35)}{10})} \tag{35}$$

$$\tau_m(V) = \frac{1000}{3.3 \exp(\frac{V+35}{20}) + \exp(\frac{-(V+35)}{20})} \tag{36}$$

where $\bar{g}_{\text{M}} = 0.07 \text{ mS/cm}^2$, $E_{\text{M}} = -100 \text{ mV}$.

Low-threshold Ca^{++} , depolarization-activated hyperpolarization and slow K^+ currents (Destexhe et al. 1993; Destexhe and Babloyantz 1991; Huguenard and Prince 1991; Wang et al. 1991)

$$I_{\text{T}} = -\bar{g}_{\text{T}} m_{\text{T}}^3 h_{\text{T}} (V - E_{\text{T}}) \tag{37}$$

$$I_{\text{h}} = \bar{g}_{\text{h}} S F (V - E_{\text{h}}) \tag{38}$$

$$I_{\text{K2}} = \bar{g}_{\text{K2}} m_{\text{K2}} (0.6h_{\text{K2,1}} + 0.4h_{\text{K2,2}}) (V - E_{\text{K}}) \tag{39}$$

where $\bar{g}_{\text{T}} = 2 \text{ mS/cm}^2$, $g_{\text{h}} = 0.02 \text{ mS/cm}^2$, $g_{\text{K2}} = 0.00005 \text{ mS/cm}^2$, $E_{\text{T}} = +120 \text{ mV}$, $E_{\text{h}} = -43 \text{ mV}$, $E_{\text{K2}} = -90 \text{ mV}$. The dynamics for the gating variables m_{T} , h_{T} , S , F , m_{K2} , $h_{\text{K2,1}}$, $h_{\text{K2,2}}$ have non-standard forms, and can be found in Table 1 of Destexhe et al. (1993).

Publisher’s note Springer Nature remains neutral with regard to jurisdictional claims in published maps and institutional affiliations.

References

Arakaki, T., Mahon, S., Charpier, S., Leblois, A., Hansel, D. (2016). The role of striatal feedforward inhibition in the maintenance of absence seizures. *Journal of Neuroscience*, 36, 9618–9623.

Beenhakker, M.P., & Huguenard, J.R. (2009). Neurons that fire together also conspire together: is normal sleep circuitry hijacked to generate epilepsy? *Neuron*, 62, 612–632.

Behrens, T.E.S., Johansen-Berg, H., Woolrich, M.W., Smith, S.M., Wheeler-Kingshott, C.A.M., Boulby, P.A., Barker, G.J., Sillery, E.L., Sheehan, K., Ciccarelli, O., Thompson, A.J., Brady, J.M., Matthews, P.M. (2003). Non-invasive mapping of connections between human thalamus and cortex using diffusion imaging. *Nature Neuroscience*, 6, 750–757.

Berkovic, S.F. (1993). Childhood absence epilepsy and juvenile absence epilepsy. In E. Wyllie (Ed.) *The treatment of epilepsy: principles and practice* (pp. 547–551). Philadelphia: Lea & Febiger.

Bouwman, B.M., Suffczynski, P., Lopes da Silva, F.H., Maris, E., Rijn, C.M. (2007). GABAergic mechanisms in absence epilepsy: a computational model of absence epilepsy simulating spike and wave discharges after vigabatrin in WAG/rj rats. *European Journal of Neuroscience*, 25, 2783–2790.

Breakspear, M., Roberts, J.A., Terry, J.R., Rodrigues, S., Mahant, N., Robinson, P.A. (2006). A unifying explanation of primary generalized seizures through nonlinear brain modeling and bifurcation analysis. *Cerebral Cortex*, 16, 1296–1313.

Chen, Y., Parker, W.D., Wang, K. (2014). The role of T-type calcium channel genes in absence seizures. *Frontiers in Neurology*, 5, 45.

Chen, M., Cao, D., Xia, Y., Yao, D. (2017). Control of absence seizures by the thalamic feed-forward inhibition. *Frontiers of Computational Neuroscience*, 11, Article 31.

Chkhenkeli, S.A., & Milton, J. (2003). Dynamic epileptic systems versus static epileptic foci. In J. Milton, & P. Jung (Eds.) *Disease, epilepsy as a dynamic* (pp. 25–36). New York: Springer.

Crick, F. (1984). Function of the thalamic reticular complex: the searchlight hypothesis. *Proceedings of the National Academy of Sciences (USA)*, 81, 4586–4590.

Crunelli, V., & Leresche, N. (2002). Childhood absence epilepsy. Genes, channels, neurons and networks. *Nature Reviews Neuroscience*, 3, 371–381.

da Silva, F.H.L., Blanes, W., Kalitzin, S., Gomez, J.P., Suffczynski, P., Velis, F.J. (2002). Epilepsies as dynamical diseases of brain systems: basic models of the transitions between normal and epileptic activity. *Epilepsia*, 44(Suppl 12), 72–83.

da Silva, F.H.L., Blanes, W., Kalitzin, S., Gomez, J.P., Suffczynski, P., Velis, F.J. (2003). Dynamical diseases of brain systems: different routes to epileptic seizures. *IEEE Transactions of Biomedical Engineering*, 50, 540–548.

Depaulis, A., & Charpier, S. (2018). Pathophysiology of absence epilepsy: Insights from genetic models. *Neuroscience Letters*, 667, 53–65.

Depaulis, A., David, O., Charpier, S. (2016). The genetic absence epilepsy rat from Strassberg as a model to decipher the neuronal and network mechanisms of generalized epilepsies. *Journal of Neuroscience Methods*, 260, 159–174.

Destexhe, A. (1998). Spike-and-wave oscillations based on the properties of GABA_B receptors. *Journal of Neuroscience*, 18, 9099–9111.

Destexhe, A. (2008). Corticothalamic feedback: a key to explain absence seizures. In I. Soltesz, & K. Staley (Eds.) *Computational neuroscience in epilepsy* (pp. 184–214). New York: Academic Press.

Destexhe, A., & Babloyantz, A. (1991). A model of the inward current I_{h} and its possible role in thalamocortical oscillations. *Neuroreport*, 4, 223–226.

Destexhe, A., Babloyantz, A., Sejnowski, T.J. (1993). Ionic mechanisms for intrinsic slow oscillations in thalamic relay neurons. *Biophysical Journal*, 65, 1538–1552.

Destexhe, A., Contreras, D., Sejnowski, T.J., Steriade, M. (1994). Modeling the control of reticular thalamic oscillations by neuromodulators. *Neuroreport*, 5, 2217–2220.

- Destexhe, A., Bal, T., McCormick, D.A., Sejnowski, T.J. (1996). Ionic mechanisms underlying synchronized oscillations and propagating waves in a model of ferret thalamic slices. *Journal of Neurophysiology*, *76*, 2049–2070.
- Destexhe, A., Contreras, D., Steriade, M. (1998). Mechanisms underlying the synchronizing action of corticothalamic feedback through inhibition of thalamic relay cells. *Journal of Neurophysiology*, *79*, 999–1016.
- Destexhe, A., Mainen, Z., Sejnowski, T., Segev, I. (1998). Kinetic models of synaptic transmission. In C. Koch (Ed.) *Methods in neuronal modeling: from synapses to networks* (pp. 1–26). Cambridge: MIT Press.
- Driver, R.D., Sasser, D.W., Slater, M.L. (1973). The equation $x'(t) = ax(t) + bx(t - \tau)$ with small delay. *American Mathematics Monthly*, *80*, 990–995.
- Eissa, T.I., Dijkstra, K., Brune, C., Emerson, R.G., van Putten, M.J.A.M., Goodman, R.R., McKhann, G.M.Jr., Schevon, C.A., van Drongelen, W., van Gils, S.A. (2017). Cross-scale effects of neural interactions during human neocortical seizure activity. *Proceedings National Academy Science (USA)*, *114*, 10761–10766.
- Ermentrout, B. (2002). *Simulating, analyzing, and animating dynamical systems: a guide to XPPAUT for researchers and students*. Philadelphia: SIAM.
- Ermentrout, B., & Terman, D.H. (2010). *Mathematical foundations of neuroscience*. New York: Springer.
- Fan, D., Liu, S., Wang, Q. (2016). Stimulus-induced epileptic spike-wave discharges in thalamocortical model with disinhibition. *Scientific Reports*, *6*, 37703.
- Foss, J., & Milton, J. (2000). Multistability in recurrent inhibitory loops arising from delay. *Journal of Neurophysiology*, *84*, 975–985.
- Foss, J., Longtin, A., Mensour, B., Milton, J. (1996). Multistability and delayed recurrent feedback. *Physical Review Letters*, *76*, 708–711.
- Foss, J., Moss, F., Milton, J. (1997). Noise, multistability and delayed recurrent loops. *Physical Review E*, *55*, 4536–4543.
- Gupta, D., Ossenblok, P., van Luijckelaar, G. (2011). Space-time network connectivity and cortical activations preceding spike wave discharges in human absence epilepsy. *Medical Biology Engineering Computation*, *49*, 555–565.
- Hashemi, M., Hutt, A., Hight, D., Sleight, S. (2017). Anesthetic action on the transmission delay between cortex and thalamus explains the beta-fuzz observed under propofol anesthesia. *PLoS ONE*, *e0179286*, 12.
- Hodgkin, A., & Huxley, A. (1952). A quantitative description of membrane current and its application to conduction and excitation in nerve. *Journal of Physiology*, *117*, 500–544.
- Hogan, T., & Sundram, M. (1989). Rhythmic auditory stimulation in generalized epilepsy. *Electroencephalography clinical Neurophysiology*, *72*, 455–458.
- Hortnagl, H., Tasan, R.O., Wieselthaler, A., Kirchmair, E., Sieghart, W., Sperk, G. (2013). Patterns of mRNA and protein expression for GABA_A receptor subunits in the mouse brain. *Neuroscience*, *236*, 345–372.
- Houssaini, K.E., Ivanov, A.I., Bernard, C., Jirsa, V.K. (2015). Seizures, refractory status epilepticus, and depolarization block as endogenous brain activities. *Physical Review E*, *91*, 010701.
- Huguenard, J.R., & Prince, D.A. (1991). Slow inactivation of a TEA-sensitive K current in acutely isolated rat thalamic relay neurons. *Journal of Neurophysiology*, *66*(4), 1316–1328.
- Huguenard, J.R., & Prince, D.A. (1992). A novel T-type current underlies prolonged Ca(2+)-dependent burst firing in GABAergic neurons of rat thalamic reticular nucleus. *Journal of Neuroscience*, *12*, 3804–3804.
- Inspurger, T. (2015). On the approximation of delayed systems by Taylor series expansion. *Journal of Computational and Nonlinear Dynamics*, *10*, 024503.
- Jirsa, V.K., Proix, T., Perdikis, D., Woodman, M.M., Wang, H., Gonzalez-Martinez, J., Bernard, C., Bénar, C., Guye, M., Chauvel, P., Bartolomei, F. (2017). The virtual patient: individualized whole-brain models of epilepsy spread. *NeuroImage*, *145*, 377–388.
- Jirsa, V.K., Stacey, W.C., Quilichini, P.P., Ivanov, A.I., Bernard, C. (2014). On the nature of seizure dynamics. *Brain: A Journal of Neurology*, *137*, 2210–2230.
- Kandel, E., Schwartz, J., Jessell, T. (2000). *Principles of neural science*. New York: McGraw-Hill.
- Koepp, M.J., Caciagli, L., Pressler, R.M., Lehnertz, K., Beniczky, S. (2016). Reflex seizures, traits, and epilepsies: from physiology to pathology. *Lancet Neurology*, *15*, 92–105.
- Kostopoulos, G.K. (2000). Spike-and-wave discharges of absence seizures as a transformation of sleep spindles: the continuing development of a hypothesis. *Clinical Neurophysiology*, *111*(Suppl. 2), S27–S38.
- Kreindler, A. (1965). *Experimental epilepsy*. New York: Elsevier.
- Kurzweil, J. (1971). Small delays don't matter. In D. Chillingworth (Ed.) *Proceedings of the symposium on differential equations and dynamical systems, lecture notes in mathematics* (pp. 47–49). New York: Springer.
- Landisman, C.E., Long, M.A., Beierlein, M., Deans, M.R., Paul, D.L., Connors, B.W. (2002). Electrical synapses in the thalamic reticular nucleus. *Journal of Neuroscience*, *22*, 1002–1009.
- Ma, J., & Wu, J. (2007). Multistability in spiking neuron models of delayed recurrent inhibitory loops. *Neural Computation*, *19*, 2124–2148.
- Mak-McCully, R.A., Rolland, M., Sargsyan, A., Gonzalez, C., Magnin, M., Chauvel, P., Rey, M., Bastuji, H., Halgren, E. (2017). Coordination of cortical and thalamic activity during non-REM sleep in humans. *Nature Communications*, *8*, 15499.
- Maljevic, S., Krampfl, K., Cobilanschi, J., Tilgen, N., Beyer, S., Weber, Y.G., Schlesinger, F., Ursu, D., Melzer, W., Cossette, P., Bufler, J., Lerche, H., Helis, A. (2006). A mutation in the GABA_A receptor α_1 -subunit is associated with absence epilepsy. *Annals of Neurology*, *59*, 983–987.
- McCormick, D.A., Wang, Z., Huguenard, J. (1993). Neurotransmitter control of neocortical neuronal activity and excitability. *Cerebral Cortex*, *3*, 387–398.
- McDougal, R.A., Morse, T.M., Carnevale, T., Marengo, L., Wang, R., Migliore, M., Miller, P.L., Shepherd, G.M., Hines, M.L. (2017). Twenty years of modelDB and beyond: building essential modeling tools for the future of neuroscience. *J Comput Neurosci.*, *42*(1), 1–10.
- McKusick, V.A. (2017). Mendelian inheritance in man: a catalogue of human genes and genetic disorders. <https://www.omin.org>.
- Meeren, H.K., Pijn, J.P., Luijckelaar, E.L., Coenen, A.M., da Silva, F.H.L. (2002). Cortical focus drives widespread corticothalamic networks during spontaneous absence seizures in rats. *Journal of Neuroscience*, *22*, 1480–1485.
- Milanowski, P., & Suffczynski, P. (2016). Seizures start without common signatures of critical transitions. *International Journal of Neurological Systems*, *26*, 1650053.
- Milton, J.G., Gotman, J., Remillard, G.M., Andermann, F. (1987). Timing of seizure recurrence in adult epileptics: a statistical analysis. *Epilepsia*, *28*, 471–478.
- Milton, J., & Jung, P. (2003). *Epilepsy as a dynamic disease*. New York: Springer.
- Milton, J., & Ohira, T. (2014). *Mathematics as a laboratory tool: dynamics, delays and noise*. New York: Springer.
- Milton, J., Wu, J., Campbell, S.A., Bélair, L. (2017). Outgrowing neurological diseases: Microcircuits, conduction delay and dynamics diseases. In P. Erdi, S. Bhattacharya, A. Cochran (Eds.) *Computational neurology - computational psychiatry: why and how?* (pp. 11–47). New York: Springer.

- Milton, J.G. (2000). Epilepsy and the multistable nervous system. In J. Walleczek (Ed.) *Self-organized biological dynamics and nonlinear control by external stimuli* (pp. 374–386). Cambridge: Cambridge University Press.
- Milton, J.G., Chkhenkeli, S.A., Towle, V.L. (2007). Andamp; A.R. McIntosh Brain connectivity and the spread of epileptic seizures. In Jirsa, V.K. (Ed.) *Handbook of brain connectivity* (pp. 477–503). New York: Springer.
- Nagaraj, V., Lee, S., Krook-Magnuson, E., Soltesz, I., Benquet, P., Irazoqui, P., Netoff, T. (2015). The future of seizure prediction and intervention: Closing the loop. *Journal of Clinical Neurophysiology*, 32, 194–206.
- Osorio, I., Frei, M.G., Sornette, D., Milton, J., Lai, Y.C. (2010). Epileptic seizures: quakes of the brain? *Physical Review E*, 82, 021919.
- Osorio, I., Zaveri, H.P., Frei, M.G., Arthurs, S. (2011). *Epilepsy: the intersection of neurosciences, biology, mathematics, engineering and physics*. New York: CRC Press.
- Paz, J.T., Bryant, A.S., Peng, K., Fenno, L., Yizhar, O., Frankel, W.N., Deisseroth, K., Huguenard, J.R. (2011). A new mode of corticothalamic transmission revealed in the Gria44^{-/-} model of absence epilepsy. *Nature Neuroscience*, 14, 1167–1173.
- Penry, J.K., Porter, R.J., Driefess, F.E. (1975). Simultaneous recording of absence seizures with videotape and electroencephalography. A study of 374 seizures in 48 patients. *Brian*, 98, 427–440.
- Pollack, P.O., Guillemain, J., Hu, E., Deransant, C., Depaulis, A., Charpier, S. (2007). Deep layer somatosensory cortical neurons initiate spike-and-wave discharges in a genetic model of absence seizures. *Journal of Neuroscience*, 27, 6590–6599.
- Powell, K.L. et al. (2009). A Cav3. 2 T-type calcium channel point mutation has splice-variant-specific effects on function and segregates with seizure expression in a polygenic rat model of absence epilepsy. *Journal of Neuroscience*, 29(2), 371–380.
- Tsakiridou, E., Bertollini, L., de Curtis, M., Avanzini, G., Pape, H. (1995). Selective increase in T-type calcium conductance of reticular thalamic neurons in a rat model of absence epilepsy. *Journal of Neuroscience*, 15(4), 3110–3117.
- Quan, A., Osorio, I., Ohira, T., Milton, J. (2011). Vulnerability to paroxysmal oscillations in delayed neural networks: A basis for nocturnal frontal lobe epilepsy? *Chaos*, 21, 047512.
- Roberts, J.A., & Robinson, P.A. (2008). Modeling absence seizure dynamics: Implications for basic mechanisms and measurement of thalamocortical and corticothalamic latencies. *Journal of Theoretical Biology*, 253, 189–201.
- Robinson, P., Rennie, C.J., Rowe, D.L. (2002). Dynamics of large-scale brain activity in normal arousal states and epileptic seizures. *Physical Review E*, 65, 041924.
- Salami, M., Itami, C., Tsumoto, T., Kimura, F. (2003). Change of conduction velocity by regional myelination yields constant latency irrespective of distance between thalamus and cortex. *Proceedings of the National Academy of Sciences (USA)*, 100, 6174–6179.
- Skinner, F.K., Bazzazi, H., Campbell, S.A. (2005). Two-cell to N-cell heterogeneous, inhibitory networks: precise linking of multistable and coherent properties. *J. Computational Neuroscience*, 18(3), 343–352.
- Soltesz, I., & Staley, K. (2008). *Computational neuroscience in epilepsy*. New York: Academic Press.
- Suffczynski, P., Kalitzin, S., Lopes da Silva, F.H. (2004). Dynamics of non-convulsive epileptic phenomena modeled by a bistable neuronal network. *Neuroscience*, 126, 467–484.
- Swadlow, H.A., & Waxman, S.G. (2012). Axonal conduction delays. *Scholarpedia*, 7(6), 1451.
- Tenney, J.R., Fujiwara, H., Horn, P.S., Jacobsen, S.E., Glaser, T.A., Rose, D.F. (2013). Focal corticothalamic sources during generalized absence seizures: a MEG study. *Epilepsy Research*, 106, 113–122.
- Traub, R.D., & Miles, R. (1991). *Neuronal networks of the hippocampus*. New York: Cambridge University Press.
- van de Kamp, C., Gawthrop, P.J., Gollee, H., Loram, I.D. (2013). Refractoriness in sustained visuo-manual control. is the refractory duration intrinsic or does it depend on external system parameters? *PLoS Computational Biology*, e1002843, 9.
- Vince, M.A. (1948). The intermittency of control movements and the psychological refractory period. *British Journal of Psychology General Section*, 38, 149–157.
- Wallace, R.H., Marini, C.V., Petrou, S., Harkin, L.A., Bowser, D.N., Panchal, R.G., Williams, D.A., Sutherland, G.R., Mulley, J.C., Scheffer, I.E., Berkovic, S.F. (2001). Mutant GABA_A receptor γ 2-subunit in childhood absence epilepsy and febrile seizures. *Nature Genetics*, 28, 49–52.
- Wang, X.J., Rinzal, J., Rogawski, M.A. (1991). A model of the T-type calcium current and the low-threshold spike in thalamic neurons. *Journal of Neurophysiology*, 66, 839–850.
- Weir, B. (1964). Spikes-wave from stimulation of reticular core. *Archives of Neurology*, 11, 209–218.
- Weiss, S.A., Banks, G.P., McKhan, G.M. Jr., Goodman, R.R., Emerson, R.G., Trevelyan, A.J., Schevon, C.A. (2013). Ictal high frequency oscillations distinguish two types of seizure territories in humans. *Brain*, 136, 3796–3808.
- Westmije, I., Ossenblok, P., Gunning, B., van Luijtelaar, G. (2009). Onset and propagation of spike and slow wave discharges in human absence epilepsy: a MEG study. *Epilepsia*, 50, 2538–2548.
- Williams, D. (1953). A study of thalamic and cortical rhythms in petit mal. *Brain: A Journal of Neurology*, 76, 50–69.
- Yang, D.-P., & Robinson, P.A. (2017). Critical dynamics of Hopf bifurcations in the corticothalamic system: Transitions from normal arousal states to epileptic seizures. *Physical Review E*, 95(4), 042410.
- Zhou, C., Ding, L., Deel, M.E., Ferrick, E.A., Emeson, R.B., Gallagher, M.J. (2015). Altered intrathalamic GABA neurotransmission in a mouse model of a human genetic epilepsy syndrome. *Neurobiology of Disease*, 73, 407–417.